A Frontal Thunderstorm With Several Multi-Cell Lines Found to Produce Energetic Preliminary Breakdown

I. Kolmašová, S. Soula, O. Santolík, T. Farges, O. Bousquet, G. Diendorfer, R. Lán, L. Uhlíř

JGR Atmospheres

RESEARCH ARTICLE
10.1029/2021JD035780

A Frontal Thunderstorm With Several Multi-Cell Lines Found to Produce Energetic Preliminary Breakdown

I. Kolmašová[1,2], S. Soula[3], O. Santolík[1,2], T. Farges[4], O. Bousquet[5], G. Diendorfer[6], R. Lán[1], and L. Uhlíř[1]

[1]Department of Space Physics, Institute of Atmospheric Physics of the Czech Academy of Sciences, Prague, Czechia, [2]Faculty of Mathematics and Physics, Charles University, Prague, Czechia, [3]Laboratoire d'Aérologie, Université de Toulouse, CNRS, OMP, UPS, Toulouse, France, [4]CEA, DAM, DIF, Arpajon Cedex, France, [5]LACy, Météo-France/CNRS/Université de La Réunion, Saint-Denis, France, [6]Department of ALDIS, OVE Service GmbH, Vienna, Austria

Key Points:

- Energetic preliminary breakdown pulses were found in broadband electromagnetic recordings from a multi-cell summer thunderstorm
- Analysis of electromagnetic and radar data placed the preliminary breakdown process in small short living cells outside or on edges of the main convective line
- Presence of strong negative charge pockets and a strong lower positive charge region inside the thundercloud could explain the observation

Correspondence to:
I. Kolmašová,
iko@ufa.cas.cz

Citation:
Kolmašová, I., Soula, S., Santolík, O., Farges, T., Bousquet, O., Diendorfer, G., et al. (2022). A frontal thunderstorm with several multi-cell lines found to produce energetic preliminary breakdown. *Journal of Geophysical Research: Atmospheres*, *127*, e2021JD035780. https://doi.org/10.1029/2021JD035780

Received 31 AUG 2021
Accepted 1 FEB 2022

Author Contributions:
Data curation: T. Farges, G. Diendorfer, R. Lán
Formal analysis: T. Farges
Methodology: S. Soula, O. Santolík
Software: L. Uhlíř
Visualization: S. Soula
Writing – original draft: S. Soula
Writing – review & editing: O. Santolík, T. Farges, O. Bousquet, G. Diendorfer

Abstract We combine electromagnetic measurements with meteorological and lightning detection data to explain an observation of unusually strong preliminary breakdown (PB) produced by a thunderstorm system that developed along the Mediterranean Coast of Southern France in the early hours of 19 June 2013. This multi-cellular storm was composed of several parallel convective lines in the NW-SE direction. Our analysis focuses on 10 sequences of energetic electromagnetic PB pulses recorded by two receivers located at different distances from this thunderstorm. The peak currents, which generated these strong PB pulses, reached −36 kA. The initial polarity of all observed energetic PB pulses confirmed the movement of the negative charge downward, as in case of PB pulses preceding negative cloud-to-ground discharges. The locations of PB pulses appeared in areas with none or very weak lightning activity. Most PB pulses were initiated in small, short-living, rapidly moving convective storm cells characterized by low reflectivity values (generally <40 dBZ), weak vertical development, and low flash density. Our findings indicate that the observed thunderstorm might possess temporary strong negatively charged pockets located above a strong positive charge region at low-level. Such charge arrangement, likely explains our observation of unusually strong PB pulses and the absence of RS pulses in electromagnetic recordings.

1. Introduction

Investigation of lightning initiation from electromagnetic signatures has started in 1950s (Clarence & Malan, 1957; Norinder & Knudsen, 1956). From that time, sequences of bipolar pulses in electromagnetic records have been intensively studied, as they are believed to accompany the initiation of the majorities of both cloud-to-ground (CG) and intracloud (IC) lightning flashes (Marshall, Schulz, et al., 2014). These pulses, which are called preliminary breakdown (PB) or initial breakdown pulses in different studies, can be detected hundreds of kilometers away from their incloud sources (Kolmašová et al., 2016; Kotovsky et al., 2016). Measurements conducted several kilometers away from the lightning initiation showed that the first PB pulse is preceded by an ionizing initiation event, followed by an initial electric field change (Marshall et al., 2019; Marshall, Stolzenburg, et al., 2014).

The PB process in the CG lightning flashes is usually followed by a stepped leader that leads to the first return stroke (RS) (Rakov & Uman, 2003 and references herein). The PB electromagnetic pulses are partially detected by lightning location networks when they produce appropriately large field pulses. Their source currents are generally weaker than the currents flowing in the RS lightning channels. The analysis of electromagnetic recordings revealed that ratios of pulse amplitudes of the strongest PB pulses in individual sequences and corresponding RS pulses could substantially differ depending on geographic locations and seasons. This ratio (PB/RS) varies from low values in tropics and subtropics (15% in Florida, USA—Zhu et al., 2016; 17% in Sri Lanka—Gomes et al., 1998; 28% in Malaysia—Baharudin, Fernando, et al., 2012; Baharudin, Noor, et al., 2012) to higher values at higher latitudes or during the winter season (47% in Hokuriku, Japan—Wu et al., 2013; 70% Albany, NY, USA—Brook, 1992; 101% in Sweden—Gomes et al., 1998). Sometimes the PB process does not evolve into a regular RS; nevertheless, the properties of these PB sequences are similar to those of the PB that precede negative CG flashes (Kolmašová et al., 2020). Such lightning events are described in the literature as "inverted IC discharges" (Chilingarian et al., 2020; Nag & Rakov, 2009; Zhang et al., 2002, 2015); "attempted CG leaders" (Nag & Rakov, 2008, 2009), "isolated breakdown pulses" (Kolmašová et al., 2018; 2020; Sharma et al., 2008),

"low-level IC flashes" (Qie et al., 2005), or "PB-type flashes" (Ma, 2017). The modeling results showed that a strong lower positive charge region (LPCR), which obstructs further propagation of the evolving discharge down to the ground, is responsible for this phenomenon (Iudin et al., 2017; Tan et al., 2014).

To understand better the lightning initiation process, electromagnetic measurements of PB sequences are occasionally combined with weather radar measurements as the properties of thunderclouds along with the composition of hydrometeors are crucial for the cloud electrification and thus also for the lightning initiation (Bousquet et al., 2015; Gurevich & Karashtin, 2013; Ribaud et al., 2016). Using the radar data, Schulz et al. (2016) found that the total rate of lightning is a better indicator of an onset of the severity of the storm (strong winds, large hails, tornadoes) then rate of CG lightning only. Increased counts than of IC lightning indicate strengthening of the updraft within the thunderstorm. MacGorman et al. (2011) found that the time delay of the first CG lightning in the strom after the first IC lightning substantially varied (0–30 min) in different geographical conditions. The study of Fuchs et al. (2015) revealed that the flash rates are sensitive to the normalized convective available potential energy (CAPE), cloud base height and concentration of aerosols. Carey and Buffalo (2007) hypothesized that broad strong updrafts and associated large liquid water contents in severe storms lead to the generation of an inverted charge structure producing increased numbers of +CG lightning. Lang and Rutledge (2011) found differences in +CG and −CG dominated cells, when +CG cells had larger volumes and were more vertically developed. Marshall and Stolzenburg (2002) introduced a model calculating the electrostatic energy in extensive electrified clouds. They found that the charge structure can constrain the types of lightning flashes, and that −CG lightning cannot occur with a lower positive charge region is absent.

Karunarathna et al. (2017) examined initiation locations of IC and CG lightning in Florida. They found that CG initiation generally occurred in a 30–45 dBZ region located beside or above the strongest radar echo and that, IC initiations were found in a 15–35 dBZ region. Lu et al. (2020) analyzed two storms occurring in the Jiangsu province, China, using a magnetic direction finder technique. The authors found that most of the azimuths of the PB pulses lied within areas of a strong (>45 dBZ) radar reflectivity value. Through comparing locations of PB pulses measured in Florida with radar reflectivity plots, Karunarathne et al. (2020) found that PBs were occurring at the edges of the high reflectivity cores in the 30–35 dBZ region. Hayashi et al. (2020) found a significant difference between storm cells producing both CG and IC lightning and only IC lightning. In their study conducted in Japan, the maximum radar reflectivity of cells producing only IC lightning reached on average 40 dBZ and was nearly by 7 dBZ lower for a cell producing both types of lightning.

In this study, we investigate the properties of unusually strong breakdown processes, including their pulse train characteristics and relevant thundercloud properties, which took place within a thunderstorm that occurred in the southern France on 19 June 2013. This analysis is based on a combination of broadband magnetic-field measurements, electric field measurements, European lightning detection network EUCLID (EUropean Cooperation for LIghtning Detection) detections as well as maps of radar reflectivity and cloud top temperatures (CTT). For the first time, we discuss the observation of energetic PB pulses, which remained isolated or were followed by weak RSs, in a broad meteorological context of thundercloud properties.

Section 2 describes the instrumental setup and datasets used in this study, while Section 3 introduces the meteorological situation. In Section 4, we present the analysis of the electromagnetic measurements, relevant EUCLID reports, and corresponding observations of the vertical profiles of the radar reflectivity, and its horizontal distribution at an altitude of 3 km together with CTT. In Sections 5 and 6, we discuss and summarize our results.

2. Data Sets

2.1. Lightning Observations

This study is principally based on the use of lightning and electromagnetic field measurements made at both near and long range of the thunderstorm. For short-range magnetic-field measurements we used the magnetic-field sensor SLAVIA (Shielded Loop Antenna with a Versatile Integrated Amplifier). The antenna loop plane was oriented vertically, at an azimuth of α_0 =235° (clockwise from the geographic North). A downward current at this azimuth with respect to the antenna induces the maximum positive response of the cosine antenna pattern. The sensor was coupled with a broadband receiver (5 kHz–37 MHz) sampling at 80 MHz. This receiver was initially developed for the TARANIS spacecraft (Blanc et al., 2007), and later adapted to ground-based measurements (Kolmašová et al., 2018, 2020). The voltage at the receiver input is proportional to magnetic field time derivative

$\frac{dB}{dt}\cos(\alpha - \alpha_0)$ for a source at an azimuth α. The waveform records are numerically integrated over time to estimate the variations of the horizontal magnetic field component $B\cos(\alpha - \alpha_0)$. Duration of recorded waveforms was set to 420 ms including a pre-trigger time of 3.5, 7, or 10.5 ms. The measurements were conducted in a quiet electromagnetic environment of an external measurement site of the Laboratoire Souterrain à Bas Bruit (LSBB), located on the summit of La Grande Montagne (1,028 m, 43.94°N, 5.48°E) close to Rustrel, France. For electric-field measurements further away from thunderstorm, we used a vertical whip antenna mounted on a mast. Received signals are sampled at 12.5 MHz, and analyzed in the frequency range 3 kHz–5 MHz. Duration of recorded waveform was 30 ms including a pre-trigger time of 6 ms. The electric-field analyzer was located at a distance of 321 km northwest from Rustrel (at 560 m, 46.1°N, 2.8°E). A detailed description of the instrumentation is given in Farges and Blanc (2011). The same receiver was used in the study of Fullekrug et al. (2013) and Kolmašová et al. (2014). The time alignment was realized by the GPS receivers connected to both receivers. Before data analysis narrow-band interferences caused by radio transmitters were removed from electromagnetic recordings by applying several narrow band-pass filters.

The European lightning location network EUCLID (www.euclid.org) provided times of occurrence, locations, polarities, peak currents, and types of discharges, which were analyzed in this study. Individual EUCLID sensors report the angle of incidence of the electromagnetic field (method called magnetic direction finding) and the time of field arrival at the sensor. An optimization algorithm is used to find a position that fits best all the available measurements. The median location accuracy for CG discharges is about 100 m (Schulz et al., 2016) as there is a clearly defined striking point, where the lightning channel attaches to the ground and the return stroke current wave starts propagating upwards. In case of IC discharges which do not have ground striking points, EUCLID provides ground level positions that fit best the measured times received from the contributing sensors. Thus the coordinates of the IC discharges mainly result from optimization algorithm finding the best fit to times and angles reported by different sensors. In case of a perfect vertical IC channel, which could be projected as a single point at the earth surface, the location accuracy of IC is the same as for CG. In any other case it will be somewhat larger, depending on the geometry of the IC lightning channel. The detection efficiency for IC discharges was relatively low as there were not sufficient number of sensors in 2013 to localize typically weaker IC discharges.

To characterize the type of the discharge, the lightning location networks identify the CG/IC differences either in the peak-to-zero times, or in combinations of waveform parameters, or in the altitude of the discharge (Kohlmann et al., 2017). The machine learning techniques (Wang et al., 2020; Zhu et al., 2021) rely on the differences in the pulse shapes. To differentiate the "IC-type" pulses, PB pulses, and the "RS-type" pulses in our study, we used our measurements of the horizontal magnetic field components and a criterion based on visual classification of their pulse waveform shapes, as described below in Section 4.1.

2.2. Other Sources of Data

CTTs are issued from the Spinning Enhanced Visible and Infrared Imager (SEVIRI) onboard the Meteosat Second Generation (MSG) satellite operated by the European Organization for the Exploitation of Meteorological Satellites (EUMETSAT). The radiometer SEVIRI scans the Earth disk to provide images in 12 spectral bands every 15 min at a spatial resolution of 0.027°, which corresponds to 3 km at the subsatellite point and about 4.5 km at the latitude of the study area (around 43°). The study area is therefore scanned four times in one hour, around 10, 25, 40, and 55 min of each hour. The thermal infrared band (IR) at ∼11–13 μm allows estimating the CTT with an accuracy generally better than ∼1°C.

Radar data used in this study were collected by the operational radar network ARAMIS (from French « Application Radar à la Météorologie Infra-Synoptique » which means Radar Application to the Meterology Infra-Synoptic). Radar reflectivity observations were composited following the approach described in Bousquet and Tabary (2014) to produce gridded reflectivity products at the spatio-temporal resolution of 1 km horizontally, 500 m vertically and 15 min from using plan position indicator (PPI) data collected during 15' volumic radar cycles. In order to account for the non-simultaneity of the measurements during each 15' period of sampling, all observations are synchronized with respect to the ending time of the period (the reader is referred to Bousquet et al., 2008 for more details about data analysis).

To analyze the meteorological conditions for the day of the storm that produced the PB pulses, we use the ERA5 reanalyzes provided by the European Centre for Medium-Range Weather Forecasts (ECMWF; available on the

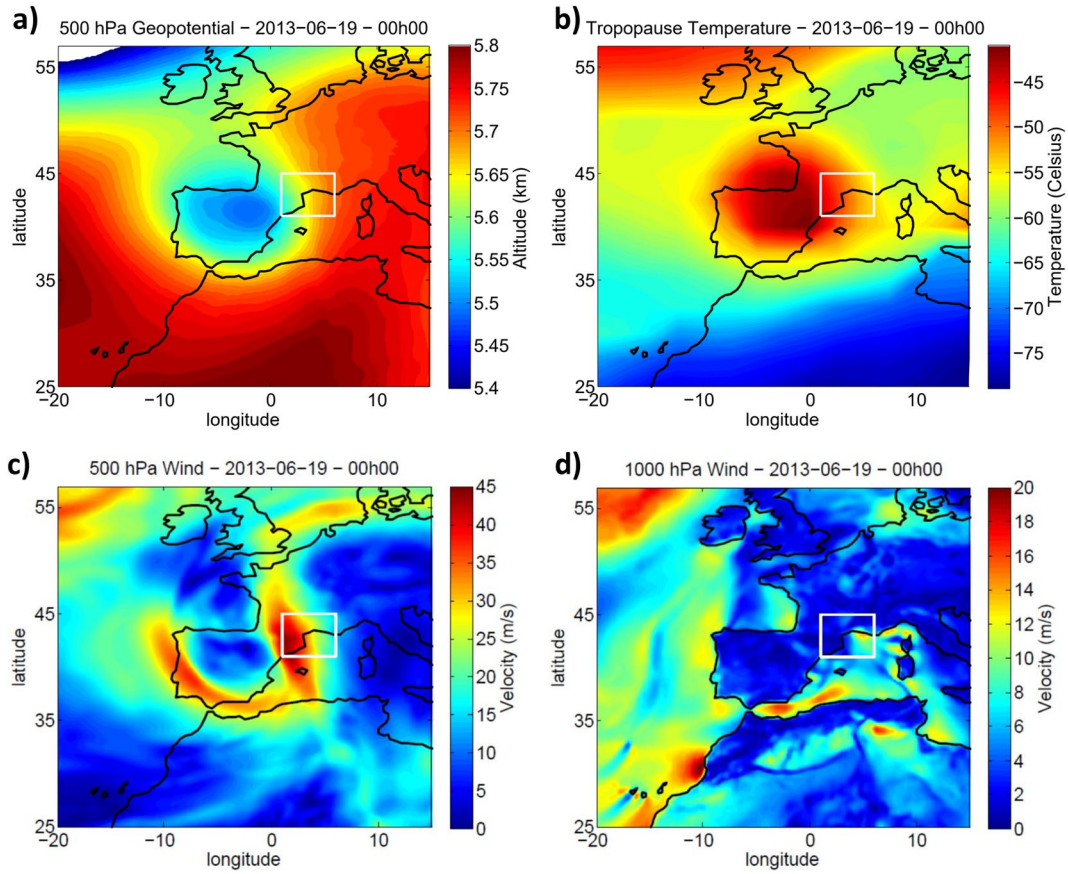

Figure 1. Description of the meteorological conditions on 19 June 2013 at 00:00 UTC, at the synoptic scale over Europe, from ERA5 reanalyzes for (a–d), and from NCEP/NCAR reanalyzes for (b): (a) Geopotential at 500 hPa with the color scale that indicates the altitude in km (b) Temperature of the tropopause in degree celsius. (c and d) Intensity of the geostrophic wind, at 500 hPa and 1,000 hPa levels, respectively, with a different scale in m s^{-1}. The white frames indicate the study area.

European Copernicus/ECMWF Data Center) to retrieve CAPE, geopotential (at 500 hPa), and horizontal wind velocity (at 1,000 and 500 hPa levels). ERA5 is based on the Integrated Forecasting System (IFS) Cy41r2 which was operational in 2016 (Hersbach et al., 2020). Furthermore, we use the NCEP/NCAR reanalyzes for the tropopause temperature which is a parameter available in the database produced thanks to a cooperation of the NCEP and the NCAR (Kalnay et al., 1996).

3. Meteorological Context

3.1. Weather Patterns at Synoptic and Regional Scales

On 19 June 2013, weather forecasts (https://www.estofex.org/) show a high probability of Deep Moist Convection (DMC) with very high CAPE values (exceeding 3,000 J kg^{-1}) over a large part of Central Europe. This was mainly due to the overlap of steep lapse rates of temperature along with high boundary layer moisture (dew points exceeding 20°C). Furthermore, an upper low initially centered over the Iberic Peninsula moved northwards above the Bay of Biscay, together with a surface cold front. It formed a cold-core low and forced a southeasterly flow over France (Figure 1). Figure 1a, which shows the altitude of the pressure level 500 hPa, highlights the cold-core low centered above northern Spain, with lower values around 5.5 km. Above the study area (1°−6°E; 41°–45°N), the altitude of the 500 hPa pressure was comprised between 5.6 and 5.7 km. A first consequence of this low is a lower altitude and a warmer temperature of the tropopause within the area, as indicated in Figure 1b. Indeed, the tropopause temperature had a maximum of −40°C within the center of the low and about −48°C above the study area. Another consequence is the air motion counterclockwise around the low, especially strong at 500 hPa level, as indicated by Figure 1c, which shows that the velocity of the geostrophic wind is maximum in the west part of

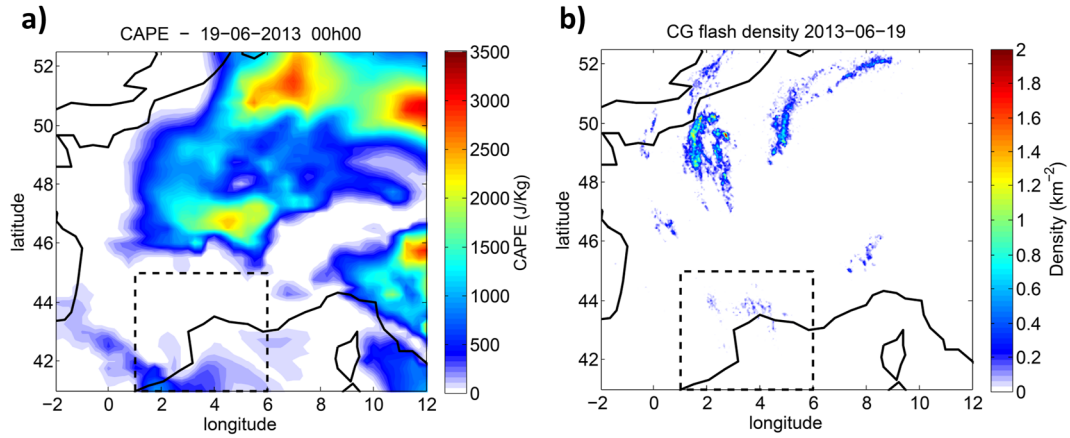

Figure 2. (a) CAPE value at the synoptic scale calculated at a resolution of 0.25° × 0.25° from ERA5 reanalysis. (b) CG lightning flash density calculated at a resolution of 0.05° × 0.05° in the same area. The flashes are reconstructed from lightning strokes detected by EUCLID in the 6-hr period 01:00–07:00 UTC. The frames in dotted line indicate the study area.

the study area with about 45 m s^{-1}. The wind at this level is generally oriented toward the north in the study area. Figure 1d shows the wind at 1,000 hPa level is much weaker in the study area with a velocity lower than 5 m s^{-1} in the western part of the study area and around 10 m s^{-1} in its eastern part. The wind shear was therefore very high between the two levels, especially in the western part of the study area.

At the regional scale, thunderstorms were expected over Northern France because of large values of CAPE and steeper mid-level lapse rates of temperature. Furthermore, the low-level convergence and the slowly translating frontal boundary was expected to favor thunderstorm initiation. Figure 2a displays the distribution of the CAPE over France on that day at 00:00 UTC. The larger values around 3,000 J kg^{-1} were mainly located over the north and the northeast of the map. This region of large CAPE values expanded over the northern part of France with values <2,000 J kg^{-1}, while another maximum was located over central France. Over southwestern France, weak mid-level lapse rates of temperature limited CAPE values around 500 J kg^{-1} over the Pyrénées range and up to 1,000 J kg^{-1} over Catalonia. The presence of very strong vertical wind shear, up to 40 m s^{-1} between 1,000 and 500 hPa levels (~0–6 km layer) in the western part of the study area, is expected to contribute to the development of thunderstorm systems of multi-cell type, which could maintain convective activity for a duration of a few hours (Markowski & Richardson, 2010).

3.2. Description of the Storm Activity

Figure 2b displays the CG flash density calculated with a resolution of 0.05° × 0.05° using EUCLID data collected within the 6-hr period 01:00–07:00 UTC; nearly 15,000 CG lightning flashes were recorded over France and in the surrounding area during this time period. The flash number was obtained from using typical grouping criteria of time and distance between CG strokes (0.5 s and 10 km, respectively, Cummins et al., 1998). The larger values of the CG flash density are located over northern France, with several areas of activity and a local maximum value close to 2 flashes km^{-2}. The study area is indicated by a frame in Figure 2 and corresponds roughly to the most southern part of France. The CG lightning flash density was low in this area with values not exceeding 0.25 flash km^{-2}. This lightning activity was produced by several thunderstorm cells, generally organized in southeast northwest oriented lines. Several lines of convective cells were simultaneously observed with the French radar network ARAMIS. The first cells were initially small with a size around 10 km in diameter and progressively, new cells developed and clustered within these lines which moved northwards at a velocity of about 50 km hr^{-1}. The convective system (see description in Section 4.3) displays a multi-cell organization including cells with moderate reflectivity values (up to 45 dBZ at low altitude). It produced lightning activity during more than 5 hr with low CG flash densities (up to 0.25 km^{-2}). The CTT of this convective system was not very cold since the minimum value detected during the period of lightning activity was −57°C. The coldest values of CTT were observed around 05:00 UTC. The properties of lightning discharges detected by EUCLID in the area of interest and their correspondence with our electromagnetic observations are described in Section 4.2.

4. Results

4.1. Analysis of Electromagnetic Waveforms

As a base line, we investigated magnetic field waveforms, since the magnetic field receiver used a broader frequency band and was located closer to the storm, allowing to distinguish more waveforms details. The level of instrumental noise and external interferences allows identifying broadband pulses exhibiting peak-to-peak amplitudes larger than 0.4 nT. The individual waveforms were analyzed to identify trains of bipolar PB pulses, IC-type pulses, and RS-type pulses. We used a simple criterion based on their pulse waveform shapes (Wang et al., 2020). An isolated bipolar pulse was considered to belong to an IC discharge if the immediately following overshoot of opposite polarity exceeded one-half of the peak amplitude of the original pulse. A sequence of bipolar pulses with hundred microsecond long interpulse time intervals was considered as a group of PB pulses. A RS-type pulse generated by a CG discharge was defined by a smaller overshoot of the opposite polarity, not reaching one-half of the peak amplitude of the original pulse. For simplicity, we will use shorter terms: RS, IC, and PB pulse in the following text. As the receiver was operating in a triggering mode, the recordings of waveform captures were predominantly triggered by the RS pulses. Nevertheless, strong PB pulses were also able to activate the trigger.

Whenever a PB train consisting of at least five bipolar pulses was visually identified in the magnetic field waveform, we searched for the same lightning phenomena in the concurrently recorded electric field waveform snapshots, and checked visually the similarity of the pulse train patterns recorded by both receivers. Additionally, the 420-ms long magnetic-field waveforms were used to examine the pulse activity following the PB trains within a period exceeding the longest previously published pre-stroke time interval between the PB process and the first RS (383 ms; Marshall, Schulz, et al., 2014).

The triggered waveforms have been recorded by the magnetic-field receiver from 3:24 to 5:56 UTC. In these waveform captures, we identified numerous isolated bipolar IC pulses, RS pulses, and sequences of bipolar PB pulses. As we focus on unusually strong PB pulses in this study, only trains of PB pulses fulfilling the following criteria were included in our data set:

1. The pulse train was found in both the magnetic and electric field recordings.
2. The pulse train was followed by a weak RS pulse (weaker than the strongest PB pulse in the corresponding PB train) or the RS pulse was not found in the 420 ms long magnetic field waveform.
3. The EUCLID information about the location and the peak current was available for at least one PB pulse within the pulse train. We have to note, that EUCLID converts the measured peak fields of PB pulses by using the same conversion factor as used and validated for CG strokes and that the PB currents might have been underestimated, as modeled by Kašpar et al. (2016).

The resulting data set consists of 10 strong PB trains, observed between 3:46 and 5:56 UT. The selected PB pulse trains were followed by an IC activity in seven cases and by weak RS pulses in the remaining three cases. Note, that the criteria did not include any meteorological condition and did not take into account the observed flash rates.

In the following, we focus on properties of the 10 trains of PB pulses, which were selected using the criteria defined above. We labeled them by letters from A-J. Three examples of magnetic- and electric-field waveforms containing typical PB trains are plotted in Figures 3a–3c. Magnetic field and electric field waveforms are respectively represented by blue and red lines. The initial polarity of electric field pulses confirmed the motion of the negative charge downward, as in case of negative CG discharges (note that we use the atmospheric electricity sign convention for the measurement of electric field that is positive downward). The polarity of the magnetic field pulses is given by the relative position of the receiving antenna to the recorded discharge. The polarity of the magnetic field waveforms shown in Figure 3 was inverted to stress the similarity of both magnetic and electric field pulse patterns. All waveforms were shifted in time to have the PB pulse with the largest peak-to-peak amplitude at the time $t = 0$. The peak amplitudes of PB pulses within the trains in Figures 3a and 3b were nearly monotonically increasing with time; they reached a maximum in a few hundreds of microseconds, and then decreased again, forming a "diamond" shape of the observed peak amplitudes. The pulses were relatively regularly distributed within the trains. Toward the end of the trains, the pulses lost their clear bipolar shapes, and became rather chaotically spaced. The envelopes of the pulse peak amplitudes within seven trains (out of 10) had a shape of a diamond as in Figures 3a and 3b. The envelopes of three remaining trains were less regular, similar to Figure 3c. The envelopes

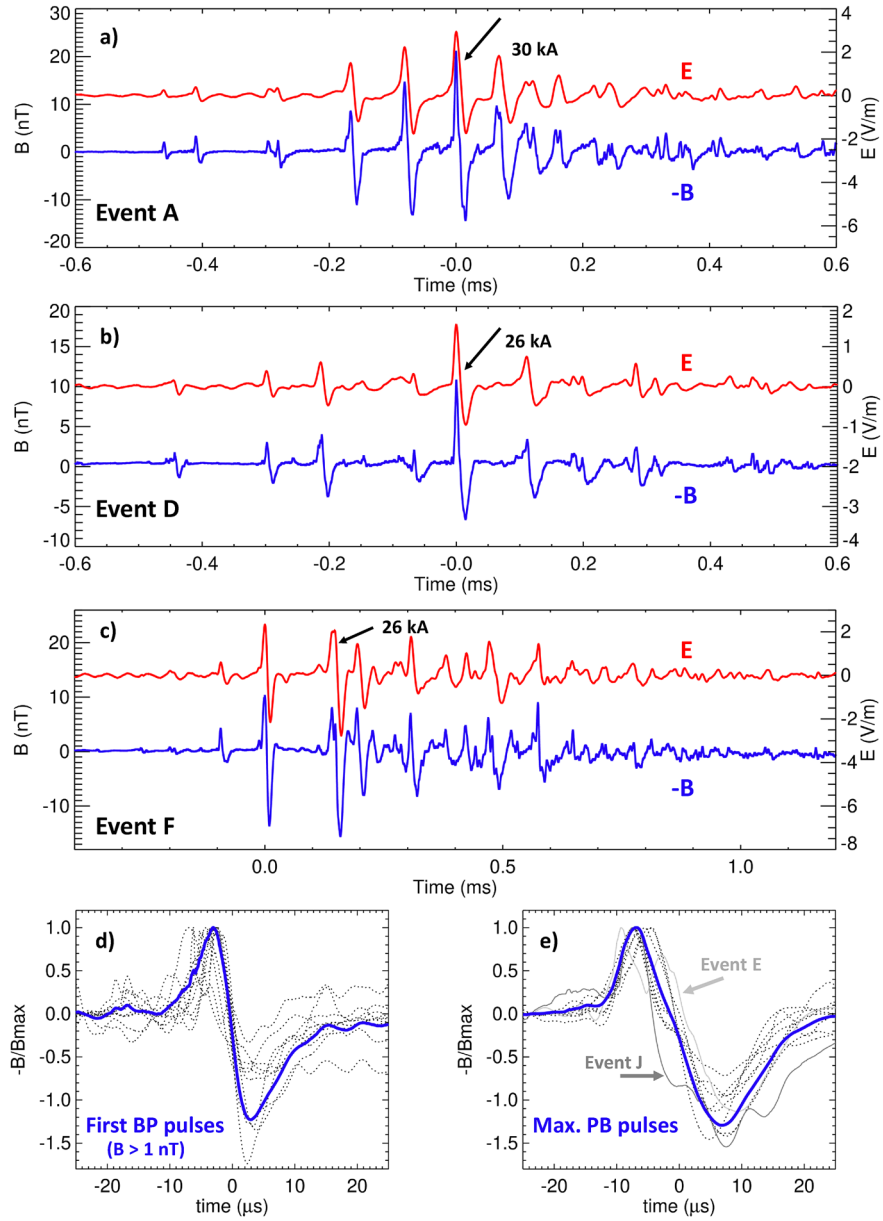

Figure 3. (a–c) Three examples of magnetic-field (blue lines) and electric-field waveforms (red lines) of trains of preliminary background (PB) pulses (events A, D, F) shifted in time to have the strongest PB at $t = 0$. PB pulses reported by EUCLID are indicated by black arrows together with their peak current estimates. (d) A normalized "small" PB pulse (calculated from the first PB pulses with an amplitude above 1 nT represented by dotted gray lines). (e) A normalized "large" pulse (calculated from the strongest PB pulses within individual PB trains represented by dotted gray lines with exception of two strongest pulses with unusual wave shapes shown by solid gray lines).

of all three trains which were followed by a weak RS had a diamond shape. Nevertheless, envelopes of other three trains which were isolated also have a shape of a diamond, so we do not see any correlation between the shape of the envelope and the presence or absence of the RS.

To estimate a range of widths of particular bipolar PB pulses detected during the thunderstorm, we have selected the first pulse with a peak-to-peak amplitude exceeding 1 nT and a pulse with the largest peak-to-peak amplitude within each magnetic-field pulse train. Two sets of 50-μs long waveform snapshots containing selected pulses were produced (Figures 3d and 3e). For each pulse, the half of the time interval between the negative and positive peaks was set as the time $t = 0$. Because of the different angles of arrival and traveled distance of individual

events, which influenced the strength of the received signal, the waveforms were normalized by their positive peak maxima. Individual pulses are plotted by black dotted lines with exception of the strongest pulses from trains E and J, which exhibited unusual shapes having two positive or negative peaks and are displayed by solid lines (light gray, train E; dark gray line, train J, indicated by arrows) in Figure 3e. The pulses plotted by blue lines show an average small pulse (Figure 3d) and an average large pulse (Figure 3e) with a similar duration of the initial polarity half-pulse of about 12 μs, and a different duration of the opposite polarity half-pulse of about 15 and 23 μs. Note that the waveshapes were not affected by the arrival angles of the received signals.

The inter-pulse time intervals between clearly distinguishable bipolar pulses in all magnetic-field trains varied from 25 to 220 μs with a mean value of 78 μs. The time between the first and the largest PB pulse varied from 260 to 650 μs with a mean value of 450 μs. To estimate the duration of the trains, we have used 10-ms long waveform snapshots starting by the first PB pulse and divided them in 100-μs long parts. Mean values of the magnetic field and standard deviations for all these parts were then estimated. Taking into account the integrated noise of the analyzer (0.14 nT given in Kolmašová & Santolík, 2013) a threshold of 0.07 nT was chosen for the absolute value of the mean and a threshold of 0.21 nT for the standard deviation. The time, when both the mean value and the standard deviation dropped permanently below their thresholds, was considered as the end of a train. Overall PB trains were found to span over 2.4 ms on average with a duration varying from 1.7 to 3.4 ms. The RS-type pulses that were found to follow the PB pulse trains A, E and G, respectively occurred 15, 81, and 20 ms after the first detectable PB pulse.

4.2. Analysis of Relevant EUCLID Detections

The time development of the thunderstorm and the flash density as detected by EUCLID are illustrated in Figure 4. The selected area (1°−6°E; 41°–45°N) covers the whole thunderstorm, which was moving to the northeast along the Mediterranean coast from 01:00 to 07:00 UTC. The lightning flash activity was recorded between 01:18 UTC and 06:35 UTC, with 1,433 reported strokes, including 927 CG strokes and 506 IC strokes. Note that the detection efficiency of EUCLID for IC discharges was still very limited in 2013. Note also that EUCLID discriminates IC and CG discharges of both polaritites, and that PB pulses—if detected-should appear in the detection list as IC discharges. Nevertheless, the variability of both IC and CG pulse shapes being enormous, the classification algorithm might get confused by non-typical waveform characteristics of detected pulses (Kohlmann et al., 2017). EUCLID provided information for the strongest PB pulses occurring within 10 trains of PB pulses (Table 1). We labeled them by letters from A to J. There were two PB pulses detected by EUCLID within the PB train G. These two PB pulses occurred at the same location 112 μs apart, belonged to two strongest pulses, and we labeled them G_a and G_b. This time delay was confirmed also by electromagnetic recordings. The EUCLID classification of the type of the discharge in Table 1, sixth column is not taking into account in our analysis as we know from the analysis of electric and magnetic waveforms, that all these PB pulses have negative IC waveform signatures. Such PB detections were misclassified as CG strokes in the CG flash density and were not considered in Figure 4a. The remaining CG strokes were grouped into 604 CG flashes using the same criteria as in Figure 2b. The CG flash density reached about 0.25 flash km^{-2}.

Figure 4c presents another representation of the time distribution of discharges detected by EUCLID including their types and peak currents. Blue crosses correspond to positive CG discharges, blue open circles show negative CG discharges, while IC discharges are represented by black dots. Although PB pulses were reported as IC, +CG and −CG in EUCLID data, we show them using red stars. Regardless of the fact that EUCLID assigned positive currents in four cases of +CG discharges related to PB pulses, we plot all of them below zero, as we were able to reveal their negative polarity from the initial polarity of PB pulses in the electric-field records. The peak currents related to PB pulses varied from 15 to 36 kA. The peak currents reported by EUCLID (indicated by arrows in Figures 3a–3c) were associated with the strongest PB pulses within trains with exception of the trains F and G. EUCLID reported the second strongest PB pulse occurring within train F and two strongest pulses occurring within train G. The peak currents belonging to three RS pulses, which were found to follow PB pulse trains, were weaker than the corresponding strongest PB pulses and reached 28, 13, and 9 kA. In three other events, EUCLID reported IC discharges following the detections related to PB pulses, in remaining four events the PB pulses detections were isolated in time with no other activity detected by EUCLID within 30 seconds. (Note that the absence of the RS or the presence of a weak RS is resulting from our selection criterium 2).

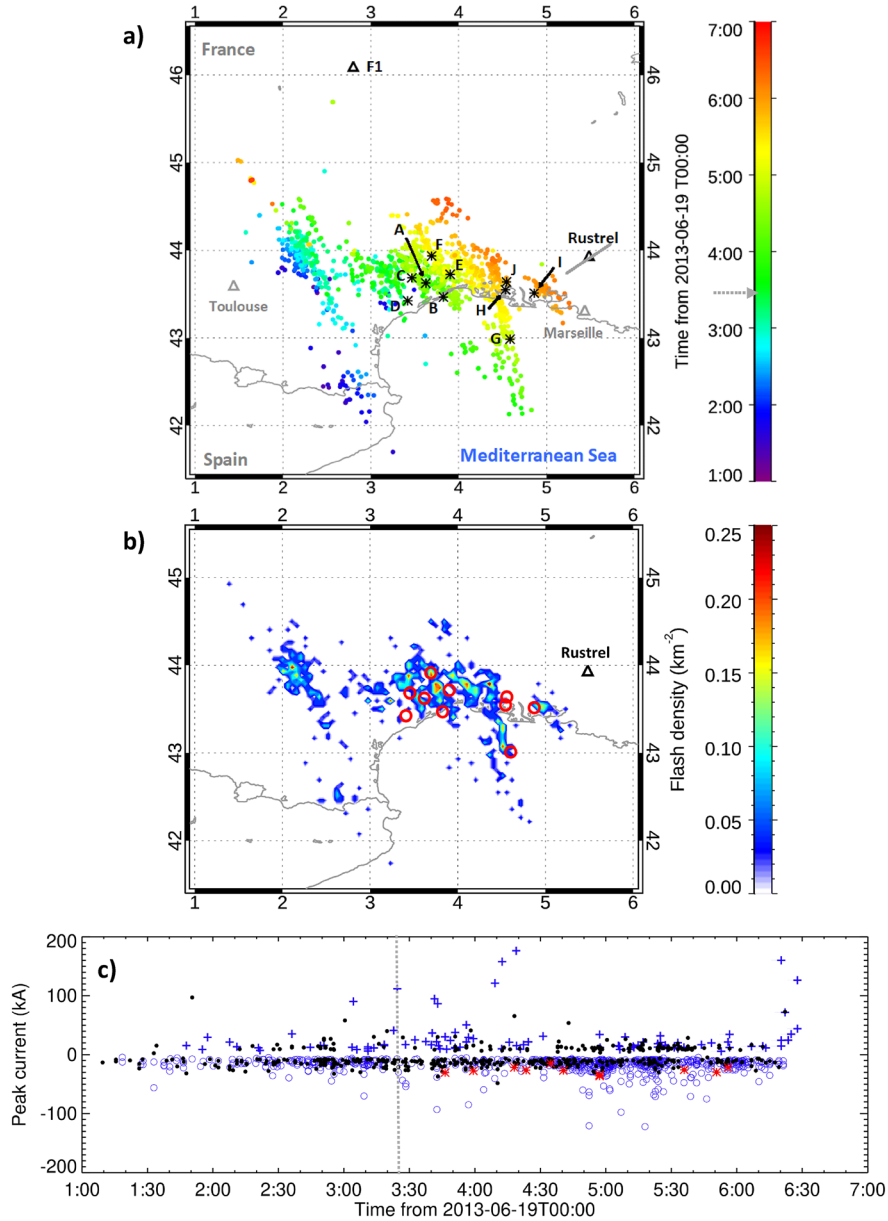

Figure 4. (a) Map showing lightning discharges detected by EUCLID color-coded by the time of their occurrence. Each bin represents an area of 25 km^2. Strong PB pulses detected by EUCLID are represented by black stars and labeled by letters. The locations of the magnetic-field receiver (Rustrel) and electric field receiver (F1) are shown by black triangles.The orientation of the magnetic loop is shown by a gray solid line. (b) Map showing the CG flash density calculated from EUCLID detections. The PB pulses detected by EUCLID are shown by red open circles. (c) Time development of the storm showing EUCLID detections together with their peak current estimates and types indicated by different symbols (positive CGs—blue crosses; negative CGs—blue open circles; ICs—black dots, strong PB pulses—red stars). The gray dotted lines show the time when the trigger of the magnetic-field receiver was activated for the first time during this storm by a strong +CG discharge.

EUCLID information indicate that the magnetic and electric field PB pulse trains were respectively measured at distances 69–176 and 253–377 km from their source lightning discharges. From this distance measurements, as the signals propagated from their source discharges to the receivers, one can independently verify the correspondence of trains measured by both receivers by checking the difference in the times of arrival of the same pulses. We found that all the analyzed pulses corresponded to the speed of light propagation within 10 μs pulse timing

Table 1
Overview of Preliminary Background (PB) Events Together With EUropean Cooperation for LIghtning Detection (EUCLID) Detections and Corresponding Cloud Top Temperature (CTT) and Radar Reflectivity

		EUCLID					Meteosat		Radar	
Train	Time UTC	Longitude (°)	Latitude (°)	Ipeak (kA)	Type	Following RS Ipeak (kA)	CTT (°C)	CTT_{min} (°C)	Z (dBZ)	Z_{max} (dBZ)
A	03:46:20	3.6258	43.6252	30	CG[a]	−28	−39	−54	32	40
B	03:59:18	3.8257	43.4664	27	CG[a]	–	−43	−54	35	40
C	04:18:05	3.4669	43.685	−21	IC	–	−39	−55	30	42
D	04:23:28	3.4198	43.4237	−26	IC	–	−38	−54	32	44
E	04:34:45	3.9035	43.7249	−15	CG[a]	−13	−45	−55	30	44
F	04:40:32	3.6916	43.9357	−27	IC	–	−43	−55	35	45
G_a	04:57:11	4.5873	42.982	34	CG[a]	−9	−50	−56.5	40	45
G_b	04:57:11	4.5846	42.9855	−36	IC		−50	−56.5	40	45
H	05:35:55	4.5331	43.5494	−26	IC	–	−48	−56.	32	45
I	05:50:45	4.8589	43.5112	−30	IC	–	−42	−56.5	30	43
J	05:55:58	4.5439	43.6384	22	CG[a]	–	−43	−57	33	45

Note. The columns indicate successively the PB event, its time of occurrence, its longitude, its latitude, the peak current, the type of discharge according to EUCLID classification, *the peak current of the following RS*, the CTT above its location, the coldest CTT in the study area at that time, the radar reflectivity value at 3 km above its location and the maximum radar reflectivity value at 3 km in the whole study area displayed in Figures 4a and 4b. Nevertheless, waveform shapes and initial polarities of these electromagnetic PB pulses confirmed that they possessed the features of pulses emitted by negative IC discharges similarly as the other PB pulses in our study. In June 2013, the detection of IC discharges by the EUCLID network was still limited, as only part of the sensors was upgraded to a new version with IC detection capability at this time (Schulz et al., 2016). The column "Type" is colored by a gray color to indicate that we did not use this information. Our IC/CG discrimination was based on the visual inspection of electromagnetic waveforms.

[a]In five cases (A, B, E, Ga, J) the PB pulses were reported by EUCLID as CG discharges.

precision. We were also able to calculate the peak-to-peak electric field amplitudes of the largest PB pulses normalized to the 100 km range assuming that the electric field amplitude is inversely proportional to the distance, without additional attenuation (Kolmašová et al., 2016). The amplitudes varied from 2.5 to 8.7 V/m reaching on average 5.9 V/m. The properties of observed PB events, and relevant EUCLID detections are summarized in Table 1.

4.3. Thundercloud Structure

In order to place our electromagnetic observations in a cloud structure context, we examine the CTT and the horizontal distribution of the radar reflectivity using horizontal cross section of the 3D reflectivity fields at a height of 3 km. These horizontal sections at 3 km altitude allow radar reflectivity values to be kept high enough to separate the convective cells which are not very developed that day, and associate PB events with the most likely cell. According to ERA5 reanalysis, the temperature at this altitude on that day is about 1° or 2°C. The vertical structure of the reflectivity field is also inferred from vertical cross-sections performed at selected locations. Figures 5–7 show these three representations at the time of occurrence of the observed strong PB pulses A, D, F, G, H, and J in the area of the convective system that produced all PB pulses. The scales of temperature and reflectivity are the same for all panels for a comparison. We superimpose in these graphs the location of the PB pulses together with those of the CG and IC discharges detected by EUCLID within a 10 min window to be as well as possible synchronized with both radar and cloud top temperature scans. The scan of the CTT above the study area is made at a given time, explicitly at 10, 25, 40, and 55 min of each hour and indicated in the CTT panels. The CG and IC discharges are represented in a time interval of 10 min straddling the times of the CTT panels, which corresponds also with the duration of the radar scan plotted in each case. In order to account for

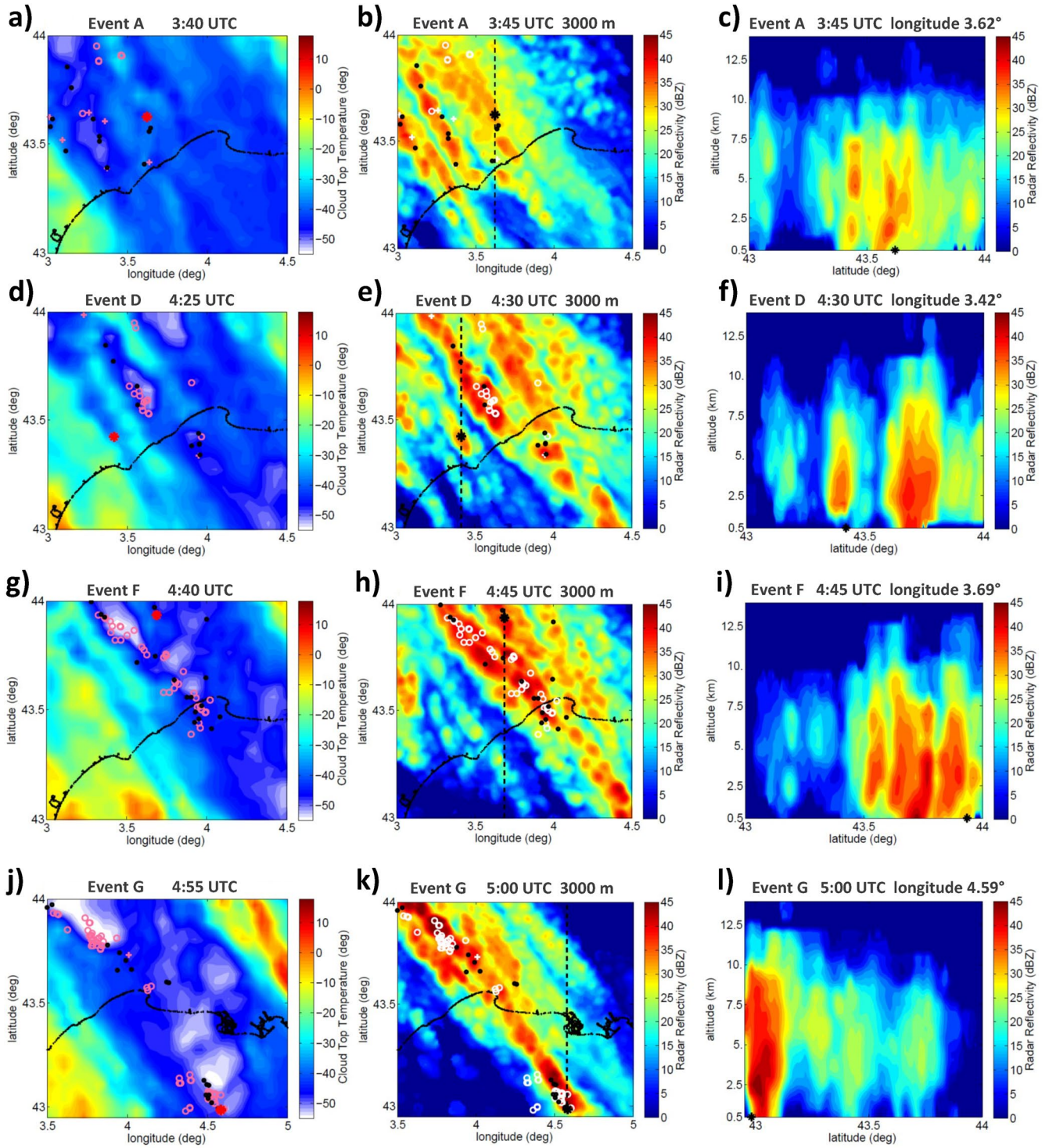

Figure 5. (a, d, g, j) CTT in Celsius at the time indicated; (b, e, h, k) horizontal cross section of radar reflectivity in dBZ at 3,000 m of altitude (from several scans made over 10 min before the time indicated); (c, f, i, l) vertical cross section of radar reflectivity along the dashed lines in (b, e, h, k). Panels (a–c) correspond with event A, panels (d–f) with event D, panels (g–i) with event F and panels (j–l) with event G. The red and black stars indicate the PB pulses location. The strokes (pulses) detected by EUCLID over 10 min 03:35–03:45 UTC for (panels a and b), 04:20–04:30 UTC for (panels d and e), 04:35–04:45 UTC for (panels g and h) and 04:50–05:00 UTC for (panels j and k) are plotted with pink and white circles for CG−, pink and white pluses for CG+ and black dots for IC.

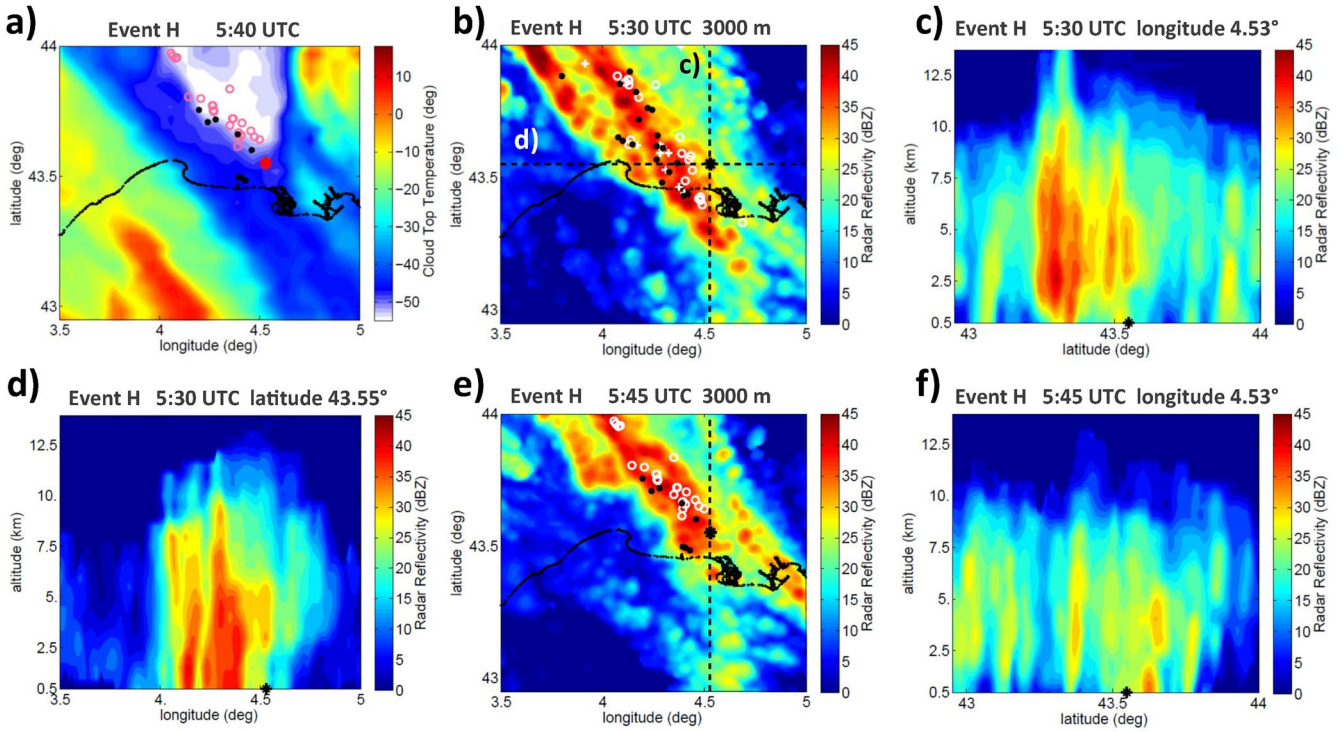

Figure 6. (a) CTT in Celsius at the time indicated; (b) horizontal cross section of radar reflectivity in dBZ at 3,000 m of altitude (from several scans made over 10 min before 05:30 UTC); (c and d) vertical cross section of radar reflectivity along the dashed lines in (b). (e) Horizontal cross section of radar reflectivity in dBZ at 3,000 m of altitude (from several scans made over 10 min before 05:45 UTC); (f) vertical cross section of radar reflectivity along the dashed lines in (e). The strokes (pulses) detected by EUCLID are plotted as in Figure 5 (05:35–05:45 UTC for panels a and e, 05:25–05:35 UTC for panel b). The PB pulses are indicated as in Figure 5.

possible errors in the synchronization of composite radar data that could arise from the fast storm motion, Table 1 indicates the minimum CTT and the maximum radar reflectivity at 3 km within the cells associated with the PB events, and for the whole system, respectively.

Figure 5 shows the plots of four cases of PB pulses from a period during which seven PB pulses were recorded (03:45–05:00 UTC) with the 10 min of lightning activity and PB pulses, for each. The storm system was characterized by northwest-southeast oriented lines of convective cells moving northwards at a speed of about 50 km hr^{-1}. Observations indicate a reinforcement of the convection over time with CTT decreasing and radar reflectivity increasing. Figures 5a and 5b display the PB event A (red and black star) and the lightning discharges over 03:35–03:45 UTC. Few discharges are produced during this period. They are located within some developing cells with CTT a little colder than −50°C (panel a) and maximum radar reflectivity of about 40 dBZ (panel b). The event A is located within a convective line with a weak vertical development, with a minimum CTT of −39°C (Figure 5a), radar reflectivity of 32 dBZ at 3 km (Figure 5b) and of 20 dBZ below 10 km (Figure 5c). This discharge is relatively isolated and is an IC pulse according its waveform shape. It was produced by a cell that has a core of reflectivity at low altitude (<2.5 km) and another one between 4 and 5 km (Figure 5c). Such structure could be related to a low dipole of charge, according to the study by Salvador et al. (2021).

Figures 5d and 5e show the discharges recorded between 04:20 and 04:30 UTC for the event D, which was detected at 04:23:28 UTC (red and black stars). These observations correspond to a more developed storm stage characterized with more discharges produced over 10 min. Most discharges were observed in the main convective line, with CTT of −54°C and reflectivity value at 3 km of 44 dBZ. However, the PB pulse D was detected alone in a small cell at the rear of the main convective line. Figure 5f shows that this cell has a weak development compared to the main line, with a CTT of about −45°C and reflectivity value of 32 dBZ at 3 km. The cell from the main line also displayed in Figure 5f at a latitude of 43.7°N is much more developed with the 20 dBZ at 11 km of height and large reflectivity values that reach the ground. The system produced even more discharges 15 min later as indicated in Figures 5g and 5h, when the PB event F was recorded. A large majority of lightning discharges are still produced within the main convective line that exhibits cells with −55°C for the coldest CTT and 45 dBZ

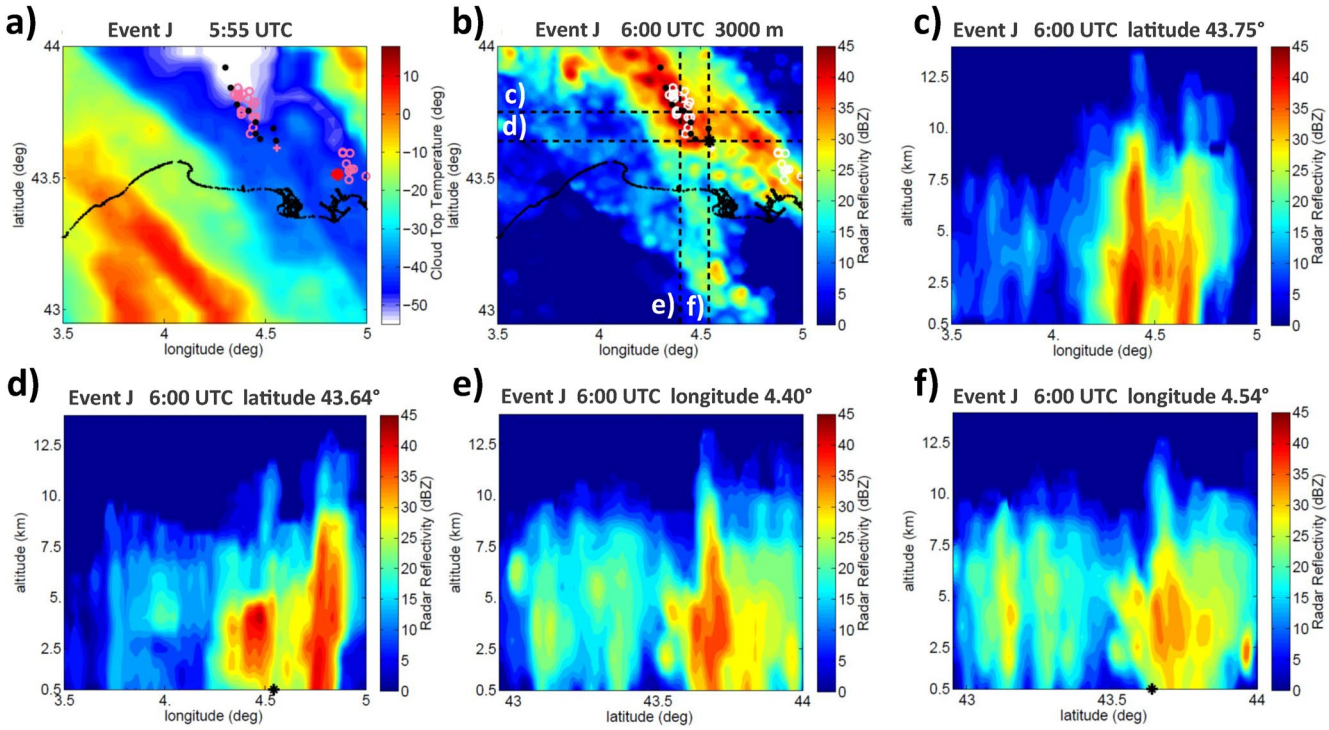

Figure 7. (a) CTT in Celsius at the time indicated; (b) horizontal cross section of radar reflectivity in dBZ at 3,000 m of altitude (from several scans made over 10 min before 06:00 UTC); (c–f) vertical cross section of radar reflectivity along the dashed lines in (b). The strokes (pulses) detected by EUCLID are plotted as in Figure 5 (05:50–06:00 UTC for panels a and b). The PB pulses are indicated as in Figure 5.

for the maximum value of the reflectivity. The cell that produced the PB event F was significantly less developed with a CTT of −43°C and a reflectivity value of 35 dBZ at 3 km. The vertical cross section of reflectivity shown in Figure 5i shows that this PB pulse seems associated with the most recent cell on the edge. Figures 5j–5l display the PB pulse G for which the area of analysis was shifted of 0.5° to the east and a little enlarged to the south in order to include the most southern part of the system. The intensity of the storm was maximum during this period as was the lightning activity in terms of flash rate (Figure 4c). The cells are now essentially organized within a single convective line. At 04:40 UTC, the CTT is colder than −55°C and the radar reflectivity reaches 45 dBZ at 3 km, in the two regions of the storm (Figures 5j and 5k) that concentrate a large majority of the lightning discharges. The PB event G is located at the edge of a cell located in the most southern area, with reflectivity value of about 40 dBZ at 3 km. It exhibits a core of reflectivity at 2.5 km with values that reach about 45 dBZ and a 20 dBZ top above 10 km of height (Figure 5l).

The PB pulse H is plotted in Figure 6 with six panels in this case. Indeed, because the PB event was produced at 05:35:55 UTC, it is difficult to associate it with a horizontal cross section of radar reflectivity and we consider two at 05:30 and 05:45 UTC. Panel a displays the CTT of the storm with a minimum value of −56°C. However, the PB pulse is out of the coldest region of the cloud top. Figures 6b and 6e display the horizontal cross section of radar reflectivity at 05:30 and 05:45 UTC, respectively. Figures 6c, 6d and 6f display three vertical cross sections according to the dashed lines in Figures 6b and 6e. For both configurations, the PB pulse is located out of the most active region of the storm, rather at its edge on east side, which is confirmed by the vertical cross sections. Indeed, the largest reflectivity values and the lightning discharges are always located to the west of the longitude of the PB location. The vertical cross sections show low values of reflectivity (30–35 dBZ) at the location of the PB event, with maximum at a height of 3–4 km and a small horizontal extent.

Figure 7 displays the last case of PB event (J) detected at 05:55:58 UTC. In this case, we plot the CTT at 05:55 UTC (panel a), the horizontal cross section of radar reflectivity at 06:00 UTC (panel b) and four vertical cross sections (panels c–f). The location of the PB pulse is out of the main convective region according to panels a and b. The four vertical cross sections, two west-east (panels c and d) and two south-north (panels e and f), allow to compare the storm structures in the vicinity of the PB pulse and in the most convective region of the storm.

We note also in this case, a weak development associated with the PB event, with no precipitation close to the ground and a low cloud top. It seems this event was produced by a weak cell in early development, or associated with very weak activity at the edge of the main storm system whose lightning activity is strongly decreasing at that time according to panel c of Figure 4.

The peak current estimated in EUCLID data varied from 22 to 36 kA for six displayed PB events, which is rather large for IC strokes. The negative polarity detected for these events suggests they may have been produced by a lower thunderstorm dipole, which consists of a negative charge layer above a positive one and tends to produce a larger proportion of IC flashes and large peak currents (Salvador et al., 2021).

5. Discussion

On 19 June 2013, a multi-cell thunderstorm produced very strong preliminary breakdown pulses over southern France, which were recorded by electric and magnetic field receivers located at a distance from about 70 to 380 km from the storm. The strong PB pulses were observed during slightly more than 2 hrs of the mature and decaying stage of the storm. That is why we assume that their appearance was not related to a known effect of the prevalence of IC discharges in the intensifying stage of thunderstorms reported by Schultz et al. (2011) or MacGorman et al. (2011). We cannot rule out that similarly strong PB pulses appeared also sooner, during the earlier stage of the thunderstorm, which was not close enough to activate the recordings of the triggered magnetic field waveform snapshots.

The properties of 10 trains of PB pulses, either isolated or followed by weak RS pulses, were analyzed. The initial polarity of the electric field PB pulses confirmed the movement of the negative charge downward, as in case of negative CG discharges. High electric field amplitudes of the largest PB pulses reached a median value of 5.4 V/m after the normalization to the 100 km. This median value exceeds three and eight times this of the largest PB pulses in negative CG flashes previously observed respectively in Austria (Marshall, Schulz, et al., 2014) and Florida (Smith et al., 2018). The time needed for a growth of the PB pulse amplitude to its peak value for the strongest pulses in our study and the average duration of the PB trains are similar to that observed in Florida (Smith et al., 2018; Zhu et al., 2016). However, the PB pulse trains observed in our study were 2–3 times longer than those previously recorded in Sweden (Sharma et al., 2008), and three times longer than those observed in Japanese winter storms (Wu et al., 2013). According to Zhang et al. (2015), at a latitude of 40°, which is similar to the location of our observations, the duration of the trains varied from 1.7 to 3.3 ms being the longest for the subset of inverted IC flashes. The inter-pulse time interval of about 80 μs found in our study is nearly identical to the average inter-pulse intervals observed by Sharma et al. (2008) in Sweden within isolated PB pulse trains and within trains, preceding negative CG flashes, respectively. It is also close to a value of 68 μs reported for inverted IC flashes observed at 40°N latitude in China (Zhang et al., 2015).

Pulse widths typically observed in our study fall within the range of average PB pulse widths of 25 and 46 μs derived from two different Florida studies (Smith et al., 2018; Zhu et al., 2016). Zhang et al. (2015) reported a huge spread of pulse width values ranging from a few microseconds to 0.2 ms.

Based on the comparison of our results with measurements conducted at different geographical locations and seasons, one can conclude that the characteristics of waveform shapes of trains of PB pulses detected in southern France did not differ from properties of PB pulses preceding usual negative CG flashes, which occur during summer storms at midlatitudes. However, despite the similar waveform characteristics, the PB pulses reported in our case study were several times stronger than these reported by Marshall, Schulz, et al. (2014) or Smith et al. (2018). The in-cloud peak currents associated with these energetic PB pulses reached on average −27 kA and might have been even underestimated, as shown by Kašpar et al. (2016). These currents were even stronger than an average peak current of −16 kA reported for negative CG lightning strokes detected in France in the same period (Schulz et al., 2016).

The CG flash density calculated over 6 hr locally exceeded 0.1 flash km^{-2} and reached a maximum density of 0.25 flash km^{-2} in a few isolated bins. The locations of PB pulses shown in Figure 4a by open red circles appeared in areas with none or very weak CG lightning activity. The only exception is event F, but the CG discharges located in the relevant bin occurred later when the main convective line crossed the area, as it can be seen in detail

in Figures 5g and 5h. Figures 5 and 6 confirm that the PB pulses were produced in regions of the storm system with a few CG discharges.

Regarding the thunderstorm structure context of these electromagnetic observations, the storm system was organized in convective lines, which moved northwards at a speed of about 50 km hr^{-1} and evolved to a main line when it was more developed. Thus, we could identify a convective line which concentrated the main lightning activity, colder CTT values up to −57°C and large radar reflectivity values up to 45 dBZ at 3 km of height. The relatively fast displacement of this convective line can partly explain the low CG flash density observed over the study area compared to another storm analyzed in Soula et al. (2014) that occurred in the same area and produced CG flash densities up to 2 flashes km^{-2}. A large majority of discharges emitting strong PB pulses, were localized out of the main convective line, in small cells at its periphery (especially cases A, C, D, E, F, H, and I). These cells produced very few lightning strokes and were much less vertically developed than the cells from the main convective line (up to about 7–8 km high). The other events were localized at the edge of the main convective line (cases B, G, and J).

The temperature of the tropopause over the study area on that day was exceptionally high, around −48°C, indicating a tropopause at low altitude (due to the presence of an upper low). Indeed, the average temperature of the tropopause at this latitude and during this season is about −65°C (Maiorana et al., 2021). Thus, the cells within the main convective line produced overshoots, with minimum CTT around −55°C (Table 1), that is, 7°–8°C colder, which corresponds to less than 1 km at this altitude (Jacobson, 2005). The radar scans showed that these cells were extending up to about 10–12 km most of time. On the contrary, the cells where most of the PB events were detected did not reach the tropopause, except for the events G and H, which were produced at the edge of the main convective line. Indeed, the minimum CTT values for the cells producing PB events range between −38°C for case D and −45°C for case E while it was −48°C and −50°C for cases H and G, respectively.

The CAPE values were low within the study area, but a strong vertical wind shear was deduced from the reanalysis in altitude to help in convection development. Consequently, the maximum vertical velocity w given by Equation 1 according to the parcel theory, was small because the CAPE values are low. In Equation 1 the velocity w is in m s^{-1} and CAPE in m^2 s^{-2} equivalent to J kg^{-1}

$$w = (2 \times \mathrm{CAPE})^{1/2} \tag{1}$$

According to Figure 2a, the CAPE values were not larger than 100 J kg^{-1} in the region where the storm developed, which provides a maximum value of 14 m s^{-1} for w. This low value can explain the existence of cells with balanced charge regions at low altitude and vertically separated by small distances. It can be understandable insofar the unique dipole has logically the same amount of charge for both polarities and with low vertical velocities the charges are not very scattered within the cloud. It corresponds with the low dipole configuration, with a lower positive charge, that tends to produce less CG flashes and larger peak current values, as described by Salvador et al. (2021) in a wide study of storms at our latitude (Northern Spain). This also means that the charging process occurs at low altitude to lead to this charging configuration, for example with the non-inductive charging process at temperatures below about −10°C which gives a positive charge to graupels (Saunders et al., 2006). If the charge poles are concentrated in small regions and close, the discharge has a small length of propagation. We cannot show the charge structure of the storm, as we have not any information from a 3D lightning detection system as a Lighting Mapping Array or from electric field soundings. Nevertheless, the radar data shows a weak vertical development and low reflectivity values for most cell structures that produced analyzed strong PB events. Based on all analyzed data we can hypothesize that a larger than usual charge at the tips of propagating leaders might have resulted in a production of very energetic PB pulses. These leaders were probably stopped or substantially weakened by the lower positive charge region that was strong enough to neutralize the negative charge above (MacGorman et al., 2011). As a result, the leaders could not propagate down to the ground or produced very weak negative CG return strokes for these convective cells.

In our study, we demonstrate an importance of combining electromagnetic measurements with detailed information about the thundercloud structure for the understanding of processes, which take place inside thunderclouds. Such detailed analysis, which includes investigation of waveform details and locates observed lighting phenomena into specific radar reflectivity regions, might be of use for performance improvements of lightning detection networks.

The lightning flash rates are directly linked to vertical air motions (Deierling & Petersen, 2008), which can explain the moderate flash rate values produced by the convective system in the study area. A majority of PB pulses was found to be initiated within convective cells of short lifetime, weak vertical development and producing few lightning discharges. The vertical structure of most of these cells shows a core of reflectivity at a few kilometers of height with a maximum value much lower than 40 dBZ and without radar echoes close to the ground. It means the cells were in a development stage and without large raindrops that could produce rainfall at the surface. It could also explain that the PB events were produced by IC discharges within these cells. Thus, the negative and positive charge regions in the small observed thunderstorm cells might be composed of temporal charged pockets and did not form large and deep layers of charge. These dense charge pockets might have occurred due to a local turbulence (Mareev & Dementyeva, 2017). Because of the weak vertical motion, positive and negative charges were not separated over a large distance, which could generate electric fields large enough to initiate IC discharges. The low radar reflectivity suggests the lack of large drops, which generally make conditions favorable for charge accumulation and for strengthening of the electric field necessary for discharge initiation (Crabb & Latham, 1974; Coquillat & Chauzy, 1994).

6. Summary

We have investigated the properties of strong preliminary breakdown pulses produced in a thunderstorm that occurred in southern France on 19 June 2013. The comprehensive analysis is based on a combination of broadband magnetic-field measurements, electric field measurements, data from European lightning detection network EUCLID, 3D cloud exploration by weather radar and cloud top temperatures issued from radiometer onboard Météosat. The weather system was observed as a multicellular storm composed of several parallel convective lines in the NW-SE direction that moved northwards and progressively intensified by forming a main convective line. We analyzed 10 sequences of energetic electromagnetic PB pulses recorded by two receivers located at different distances from this storm system. The polarity of all these energetic PB pulses corresponded to the downward motion of a negative charge, as in the case of PB pulses preceding negative CG discharges. The peak currents which generated these strong PB pulses, were estimated up to −36 kA by EUCLID. The locations of the PB pulses were in areas with none or very weak lightning activity, while return stroke pulses were found to be very weak or absent in electromagnetic recordings. Most of the PB events were initiated out of the main convective cores. Thus, they were produced in small, short-living, rapidly moving convective cells characterized by low reflectivity values (maximum reflectivity lower than 40 dBZ), weak vertical development (cloud top lower than 10 km), and low flash rate. Our interpretation is based on the presence of temporary strong negatively charged pockets located above a strong positive charge region at low-level, within these thunderclouds. Such charge arrangement, later carried down by precipitation, likely explains our observation of unusually strong PB pulses and the absence of RS pulses in electromagnetic recordings. In our study, we demonstrate an importance of combining electromagnetic measurements with detailed information about the thundercloud structure for the understanding of processes, which take place inside thunderclouds. The results are based on too small data set to be statistically significant, but our method based on a thorough inspection of electromagnetic waveforms in combination with investigation of corresponding meteorological scenarios can be used for performance improvements of lightning detection networks.

Data Availability Statement

The electromagnetic-field data are available on https://data.mendeley.com/datasets/t3kgbkd996/1, doi:10.17632/t3kgbkd996.1.

Acknowledgments
The work of I. Kolmašová, and O. Santolík, R. Lán, and L. Uhlíř was supported by the GACR grant 20–09671S and by the European Regional Development Fund-Project CRREAT (CZ.02.1.01/0.0/0.0/15_003/0000481). The authors thank Laboratoire Souterrain a Bas Bruit, UNS/UAPV/CNRS, Rustrel, France, and the Director S. Gaffet, for usage of their facility at La Grande Montagne for our receiving station. The authors thank the French AERIS/ICARE Data and Services Center which provided MSG/SEVIRI data for cloud top temperature. They thank also the European Copernicus/ECMWF Data Center, the US NCEP/NCAR and NOAA for providing meteorological reanalysis (CAPE: https://cds.climate.copernicus.eu/cdsapp#!/dataset/reanalysis-era5-single-levels?tab=form; geopotential, wind: https://cds.climate.copernicus.eu/cdsapp#!/dataset/reanalysis-era5-pressure-levels; tropopause temperature: https://psl.noaa.gov/data/gridded/data.ncep.reanalysis.html). The authors thank the French company Météorage which provided a part of the lightning data.

References

Baharudin, Z. A., Fernando, M., Noor, A. A., Mäkelä, J. S., Rahman, M., & Cooray, V. (2012). Electric field changes generated by the preliminary breakdown for the negative cloud-to-ground lightning ashes in Malaysia and Sweden. *Journal of Atmospheric and Solar-Terrestrial Physics*, *84–85*, 15–24. https://doi.org/10.1016/j.jastp.2012.04.009

Baharudin, Z. A., Noor, A. A., Fernando, M., Cooray, V., & Mäkelä, J. S. (2012). Comparative study on preliminary breakdown pulse trains observed in Johor, Malaysia and Florida, USA. *Atmospheric Research*, *117*, 111–121. https://doi.org/10.1016/j.atmosres.2012.01.012

Blanc, E., Lefeuvre, F., Roussel-Dupré, R., & Sauvaud, J. (2007). TARANIS: A microsatellite project dedicated to the study of impulsive transfers of energy between the Earth atmosphere, the ionosphere, and the magnetosphere. *Advances in Space Research*, *40*(8), 1268–1275. https://doi.org/10.1016/j.asr.2007.06.037

Bousquet, O., Berne, A., Delanoe, J., Dufournet, Y., Gourley, J. J., Van-Baelen, J., et al. (2015). Multifrequency radar observations collected in southern France during HyMeX-SOP1. *Bulletin of the American Meteorological Society*, *96*(2), 267–282. https://doi.org/10.1175/bams-d-13-00076.1

Bousquet, O., & Tabary, P. (2014). Development of a nationwide real-time 3-D wind and reflectivity radar composite in France. *Quarterly Journal of the Royal Meteorological Society*, *140*, 611–625. https://doi.org/10.1002/qj.2163

Bousquet, O., Tabary, P., & Parent du Châtelet, J. (2008). Operational multiple-Doppler wind retrieval inferred from long-range radial velocity measurements. *Journal of Applied Meteorology and Climatology*, *47*(11), 2929–2945.

Brook, M. (1992). Breakdown electric fields in winter storms. *Journal of Atmospheric Electricity*, *12*, 47–52. https://doi.org/10.1541/jae.12.47

Carey, L. D., & Buffalo, K. M. (2007). Environmental control of cloud-to-ground lightning polarity in severe storms. *Monthly Weather Review*, *135*, 1327–1353. https://doi.org/10.1175/MWR3361.1

Chilingarian, A., Khanikyants, Y., Rakov, V. A., & Soghomonyan, S. (2020). Termination of thunderstorm-related bursts of energetic radiation and particles by inverted intracloud and hybrid lightning discharges. *Atmospheric Research*, *233*, 104713. https://doi.org/10.1016/j.atmosres.2019.104713

Clarence, N. D., & Malan, D. J. (1957). Preliminary discharge processes in lightning ashes to ground. *Quarterly Journal of the Royal Meteorological Society*, *83*, 161–172. https://doi.org/10.1002/qj.49708335603

Coquillat, S., & Chauzy, S. (1994). Corona emission from raindrops in strong electric fields as a possible discharge initiation: Comparison between horizontal and vertical field configurations. *Journal of Geophysical Research*, *99*, 16897–16905. https://doi.org/10.1029/94jd00818

Crabb, J. A., & Latham, J. (1974). Corona from colliding drops as a possible mechanism for the triggering of lightning. *The Quarterly Journal of the Royal Meteorological Society*, *100*, 191–202. https://doi.org/10.1002/qj.49710042406

Cummins, K. L., Murphy, M. J., Bardo, E. A., Hiscox, W. L., Pyle, R. B., & Pifer, A. E. (1998). NLDN'95, A combined TOA/MDF technology upgrade of the US National Lightning Detection Network. *Journal of Geophysical Research*, *103*, 9035–9044. https://doi.org/10.1029/98JD00153

Deierling, W., & Petersen, W. A. (2008). Total lightning activity as an indicator of updraft characteristics. *Journal of Geophysical Research*, *113*, D16210. https://doi.org/10.1029/2007jd009598

Farges, T., & Blanc, E. (2011). Lightning and TLE electric fields and their impact on the ionosphere. *Comptes Rendus Physique*, *12*, 171–179. https://doi.org/10.1016/j.crhy.2011.01.013

Fuchs, B. R., Rutledge, S. A., Bruning, E. C., Pierce, J. R., Kodros, J. K., Lang, T. J., et al. (2015). Environmental controls on storm intensity and charge structure in multiple regions of the continental United States. *Journal of Geophysical Research: Atmosphere*, *120*, 6575–6596. https://doi.org/10.1002/2015JD023271

Fullekrug, M., Kolmasova, I., Santolik, O., Farges, T., Bor, J., Bennett, A., et al. (2013). Electron acceleration above thunderclouds. *Environmental Research Letters*, *8*, 035027. https://doi.org/10.1088/1748-9326/8/3/035027

Gomes, C., Cooray, V., & Jayaratne, C. (1998). Comparison of preliminary breakdown pulses observed in Sweden and Sri Lanka. *Journal of Atmospheric and Solar-Terrestrial Physics*, *60*, 975–979. https://doi.org/10.1016/s1364-6826(98)00007-8

Gurevich, A. V., & Karashtin, A. N. (2013). Runaway breakdown and hydrometeors in lightning initiation. *Physical Review Letters*, *110*, 185005. https://doi.org/10.1103/PhysRevLett.110.185005

Hayashi, S., Nakaike, C., & Fujibe, F. (2020). Radar characteristics of summer thunderstorms in the Kanto Plain of Japan with and without cloud-to-ground lightning. *Meteorology and Atmospheric Physics*, *133*, 233–244. https://doi.org/10.1007/s00703-020-00748-z

Hersbach, H., Bell, B., Berrisford, P., Hirahara, S., Horányi, A., Muñoz-Sabater, J., et al. (2020). The ERA5 global reanalysis. *Quarterly Journal of the Royal Meteorological Society*, *146*, 1999–2049. https://doi.org/10.1002/qj.3803

Iudin, D. I., Rakov, V. A., Mareev, E. A., Iudin, F. D., Syssoev, A. A., & Davydenko, S. S. (2017). Advanced numerical model of lightning development: Application to studying the role of LPCR in determining lightning type. *Journal of Geophysical Research: Atmosphere*, *122*, 6416–6430. https://doi.org/10.1002/2016JD026261

Jacobson, M. Z. (2005). *Fundamentals of Atmospheric Modeling*. (2nd ed., Vol. 9780521839). Cambridge University Press. https://doi.org/10.1017/CBO9781139165389

Kalnay, E., Kanamitsu, M., Kistler, R., Collins, W., Deaven, D., Gandin, L., et al. (1996). The NCEP/NCAR 40-year reanalysis project. *Bulletin of the American Meteorological Society*, *77*(3), 4372–471. https://doi.org/10.1175/1520-0477(1996)077<0437:tnyrp>2.0.co;2

Karunarathna, N., Marshall, S. K., & Stolzenburg, M. (2017). Initiation locations of lightning flashes relative to radar reflectivity in four small Florida thunderstorms. *Journal of Geophysical Research: Atmosphere*, *122*, 6565–6591. https://doi.org/10.1002/2017jd026566

Karunarathne, N., Marshall, T. C., Karunarathne, S., & Stolzenburg, M. (2020). Studying sequences of initial breakdown pulses in cloud-to-ground lightning flashes. *Journal of Geophysical Research: Atmospheres*, *125*, e2019JD032104. https://doi.org/10.1029/2019JD032104

Kašpar, P., Santolík, O., Kolmašová, I., & Farges, T. (2016). A model of preliminary breakdown pulse peak currents and their relation to the observed electric field pulses. *Geophysical Research Letters*, *43*, 596–603. https://doi.org/10.1002/2016GL071483

Kohlmann, H., Schulz, W., & Pedeboy, S. (2017). Evaluation of EUCLID IC/CG classification performance based on ground-truth data. In *2017 international symposium on lightning protection (XIV SIPDA)* (p. 35–41). IEEE. https://doi.org/10.1109/SIPDA.2017.8116896

Kolmašová, I., & Santolík, O. (2013). Properties of unipolar magnetic field pulse trains generated by lightning discharges. *Geophysical Research Letters*, *40*, 1637–1641. https://doi.org/10.1002/grl.50366

Kolmašová, I., Santolík, O., Defer, E., Kašpar, P., Kolínská, A., Pedeboy, S., & Coquillat, S. (2020). Two propagation scenarios of isolated breakdown lightning processes in failed negative cloud-to-ground flashes. *Geophysical Research Letters*, *47*, e2020GL090593. https://doi.org/10.1029/2020GL090593

Kolmašová, I., Santolík, O., Defer, E., Rison, W., Coquillat, S., Pedeboy, S., et al. (2018). Lightning initiation: Strong VHF radiation sources accompanying preliminary breakdown pulses during lightning initiation. *Scientific Reports*, *8*, 3650. https://doi.org/10.1038/s41598-018-21972-z

Kolmašová, I., Santolík, O., Farges, T., Cummer, S. A., Lán, R., & Uhlíř, L. (2016). Subionospheric propagation and peak currents of preliminary breakdown pulses before negative cloud-to-ground lightning discharges. *Geophysical Research Letters*, *43*, 1382–1391. https://doi.org/10.1002/2015GL067364

Kolmašová, I., Santolík, O., Farges, T., Rison, W., Lán, R., & Uhlíř, L. (2014). Properties of the unusually short pulse sequences occurring prior to the first strokes of negative cloud-to-ground lightning flashes. *Geophysical Research Letters*, *41*, 5316–5324. https://doi.org/10.1002/2014GL060913

Kotovsky, D. A., Moore, R. C., Zhu, Y., Tran, M. D., Rakov, V. A., Pilkey, J. T., et al. (2016). Initial breakdown and fast leaders in lightning discharges producing long-lasting disturbances of the lower ionosphere. *Journal of Geophysical Research: Space Physics*, *121*, 5794–5804. https://doi.org/10.1002/2015JA022266

Lang, T. J., & Rutledge, S. A. (2011). A framework for the statistical analysis of large radar and lightning datasets: Results from STEPS 2000. *Monthly Weather Review*, *139*, 2536–2551. https://doi.org/10.1175/MWR-D-10-05000.1

Lu, Z., Qiu, S., Wang, R., Shi, L., & Zhang, P. (2020). Orientation of initial breakdown pulses and leader discharges by magnetic direction finder. *Journal of Geophysical Research: Atmospheres*, *125*, e2019JD031407. https://doi.org/10.1029/2019JD031407

Ma, D. (2017). Characteristic pulse trains of preliminary breakdown in four isolated small thunderstorms. *Journal of Geophysical Research: Atmosphere*, *122*, 3361–3373. https://doi.org/10.1002/2016JD025899

MacGorman, D. R., Apostolakopoulos, I. R., Lund, N. R., Demetriades, N. W. S., Murphy, M. J., & Krehbiel, P. R. (2011). The timing of cloud-to-ground lightning relative to total lightning activity. *Monthly Weather Review*, *139*, 3871–3886. https://doi.org/10.1175/MWR-D-11-00047.1

Maiorana, C., Marisaldi, M., Füllekrug, M., Soula, S., Lapierre, J., Mezentsev, A., et al. (2021). Observation of terrestrial gamma-ray flashes at mid latitude. *Journal of Geophysical Research: Atmospheres*, *126*, e2020JD034432. https://doi.org/10.1029/2020JD034432

Mareev, E. A., & Dementyeva, S. O. (2017). The role of turbulence in thunderstorm, snowstorm, and dust storm electrification. *Journal of Geophysical Research: Atmospheres*, *122*, 6976–6988. https://doi.org/10.1002/2016JD026150

Markowski, P., & Richardson, Y. (2010). *Mesoscale meteorology in midlatitudes*. John Wiley & Sons. https://doi.org/10.1002/9780470682104

Marshall, T., Bandara, S., Karunarathne, N., Karunarathne, S., Kolmasova, I., Siedlecki, R., & Stolzenburg, M. (2019). A study of lightning flash initiation prior to the first initial breakdown pulse. *Atmospheric Research*, *217*, 10–23. https://doi.org/10.1016/j.atmosres.2018.10.013

Marshall, T., Schulz, W., Karunarathna, N., Karunarathne, S., Stolzenburg, M., Vergeiner, C., & Warner, T. (2014). On the percentage of lightning flashes that begin with initial breakdown pulses. *Journal of Geophysical Research: Atmosphere*, *119*, 445–460. https://doi.org/10.1002/2013JD020854

Marshall, T., Stolzenburg, M., Karunarathna, N., & Karunarathne, S. (2014). Electromagnetic activity before initial breakdown pulses of lightning. *Journal of Geophysical Research: Atmosphere*, *119*, 12574–12558. https://doi.org/10.1002/2014JD022155

Marshall, T. C., & Stolzenburg, M. (2002). Electrical energy constraints on lightning. *Journal of Geophysical Research*, *107*. https://doi.org/10.1029/2000JD000024

Nag, A., & Rakov, V. A. (2008). Pulse trains that are characteristic of preliminary breakdown in cloud-to-ground lightning but are not followed by return stroke pulses. *Journal of Geophysical Research*, *113*, D01102. https://doi.org/10.1029/2007jd008489

Nag, A., & Rakov, V. A. (2009). Some inferences on the role of lower positive charge region in facilitating different types of lightning. *Geophysical Research Letters*, *36*, L05815. https://doi.org/10.1029/2008GL036783

Norinder, H., & Knudsen, E. (1956). Pre discharges in relation to subsequent lightning strokes. *Arkiv foer Geofysik*, *2*(27), 551–571.

Qie, X., Zhang, T., Chen, C., Zhang, G., Zhang, T., & Wei, W. (2005). The lower positive charge center and its effect on lightning discharges on the Tibetan Plateau. *Geophysical Research Letters*, *32*, L05814. https://doi.org/10.1029/2004GL022162

Rakov, V. A., & Uman, M. A. (2003). *Lightning—Physics and effects*. Cambridge University Press.

Ribaud, J.-F., Bousquet, O., & Coquillat, S. (2016). Relationships between total lightning activity, microphysics and kinematics during the 24 September 2012 HyMeX bow-echo system. *Quarterly Journal of the Royal Meteorological Society*, *142*, 298–309. https://doi.org/10.1002/qj.2756

Salvador, A., Pineda, N., Montanyà, J., López, J. A., & Solà, G. (2021). Thunderstorm charge structures favouring cloud-to-ground lightning. *Atmospheric Research*, *257*, 105577. https://doi.org/10.1016/j.atmosres.2021.105577

Saunders, C. P. R., Bax-Norman, H., Emersic, C., Avila, E. E., & Castellano, N. E. (2006). Laboratory studies of the effect of cloud conditions on graupel/crystal charge transfer in thunderstorm electrification. *Quarterly Journal of the Royal Meteorological Society*, *132*, 2653–2673. https://doi.org/10.1256/qj.05.218

Schultz, C. J., Petersen, W. A., & Carey, L. D. (2011). Lightning and severe weather: A comparison between total and cloud-to-ground lightning trends. *Weather and Forecasting*, *26*, 744–755. https://doi.org/10.1175/WAF-D-10-05026.1

Schulz, W., Diendorfer, G., Pedeboy, S., & Poelman, D. R. (2016). The European Lightning Location System EUCLID—Part 1: Performance analysis and validation. *Natural Hazards and Earth System Sciences*, *16*, 595–605. https://doi.org/10.5194/nhess-16-595-2016

Sharma, S. R., Cooray, V., & Fernando, M. (2008). Isolated breakdown activity in Swedish lightning. *Journal of Atmospheric and Solar-Terrestrial Physics*, *70*, 1213–1221. https://doi.org/10.1016/j.jastp.2008.03.003

Smith, E. M., Marshall, T. C., Karunarathne, S., Siedlecki, R., & Stolzenburg, M. (2018). Initial breakdown pulse parameters in intracloud and cloud-to-ground lightning flashes. *Journal of Geophysical Research: Atmospheres*, *123*, 2129–2140. https://doi.org/10.1002/2017JD027729

Soula, S., Iacovella, F., van der Velde, O., Montanyà, J., Füllekrug, M., Farges, T., et al. (2014). Multi-instrumental analysis of large sprite events and their producing storm in southern France. *Atmospheric Research*, *135*, 415–431. https://doi.org/10.1016/j.atmosres.2012.10.004

Tan, Y., Tao, S., Liang, Y., & Zhu, B. (2014). Numerical study on relationship between lightning types and distribution of space charge and electric potential. *Journal of Geophysical Research: Atmosphere*, *109*, 1003–1014. https://doi.org/10.1002/2013JD019983

Wang, J., Huang, Q., Ma, Q., Chang, S., He, J., Wang, H., et al. (2020). Classification of VLF/LF lightning signals using sensors and deep learning methods. *Sensors*, *20*(4), 1030. https://doi.org/10.3390/s20041030

Wu, T., Takayanagi, Y., Funaki, T., Yoshida, S., Ushio, T., Kawasaki, Z.-I., et al. (2013). Preliminary breakdown pulses of cloud-to-ground lightning in winter thunderstorms in Japan. *Journal of Atmospheric and Solar-Terrestrial Physics*, *102*, 91–98. https://doi.org/10.1016/j.jastp.2013.05.014

Zhang, Y., Krehbiel, P. R., & Liu, X. (2002). Polarity inverted intracloud discharges and electric charge structure of thunderstorm. *Chinese Science Bulletin*, *47*(20), 1725–1729. https://doi.org/10.1007/bf03183317

Zhang, Y., Zhang, Y., Zheng, D., & Lu, W. (2015). Preliminary breakdown, following lightning discharge processes and lower positive charge region. *Atmospheric Research*, *161*, 52–56. https://doi.org/10.1016/j.atmosres.2015.03.017

Zhu, Y., Bitzer, P., Rakov, V., & Ding, Z. (2021). A machine-learning approach to classify cloud-to-ground and intracloud lightning. *Geophysical Research Letters*, *48*, e2020GL091148. https://doi.org/10.1029/2020GL091148

Zhu, Y., Rakov, V. A., & Tran, M. D. (2016). A study of preliminary breakdown and return stroke processes in high-intensity negative lightning discharges. *Atmosphere*, *7*. https://doi.org/10.3390/atmos7100130